THE ASTROPHYSICAL JOURNAL, 520:149–157, 1999 July 20

CO AND C_2 ABSORPTION TOWARD W40 IRS 1a

R. YOUNG SHUPING AND THEODORE P. SNOW
Center for Astrophysics and Space Astronomy, University of Colorado, Boulder, CO 80309-0389
RICHARD CRUTCHER
Department of Astronomy, University of Illinois, 205 Astronomy Building, 1002 West Green Street, Urbana, IL 61801
AND
BARRY L. LUTZ
Department of Physics and Astronomy, Northern Arizona University, Box 6010, Flagstaff, AZ 86011-6010
Received 1998 May 21; accepted 1999 March 1

ABSTRACT

The H II region W40 harbors a small group of young, hot stars behind roughly 9 mag of visual extinction. We have detected gaseous carbon monoxide (CO) and diatomic carbon (C_2) in absorption toward the star W40 IRS 1a. The $J = 2$–0 R0, R1, and R2 lines of ^{12}CO at 2.3 μm were measured using the CSHELL on the NASA Infrared Telescope Facility (with upper limits placed on R3, R4, and R5) yielding an N_{CO} of $(1.1 \pm 0.2) \times 10^{18}$ cm^{-2}. Excitation analysis indicates $T_{kin} > 7$ K. The Phillips system of C_2 transitions near 8775 Å was measured using the Kitt Peak 4 m telescope and echelle spectrometer. Radiative pumping models indicate a total C_2 column density of $(7.0 \pm 0.4) \times 10^{14}$ cm^{-2}, two excitation temperatures (39 and 126 K), and a total gas density of $n \sim 250$ cm^{-3}. The CO ice band at 4.7 μm was not detected, placing an upper limit on the CO depletion of $\delta < 1\%$. We postulate that the sight line has multiple translucent components and is associated with the W40 molecular cloud. Our data for W40 IRS 1a, coupled with other sight lines, shows that the ratio of CO/C_2 increases from diffuse through translucent environs. Finally, we show that the hydrogen-to-dust ratio seems to remain constant from diffuse to dense environments, whereas the CO-to-dust ratio apparently does not.

Subject headings: dust, extinction — infrared: ISM: lines and bands — ISM: abundances — ISM: clouds — ISM: individual (W40) — ISM: molecules

1. INTRODUCTION

Molecular species are useful diagnostics for understanding the physics and chemistry of the interstellar medium (ISM) and have been studied in various ways for many years. Most molecules are observed in dense molecular clouds via rotational emission lines in the radio band. These emission studies are indispensable to our understanding of Galactic ecology and the ISM: they yield maps of dense regions, have very high spectral (velocity) resolution, and allow us to study complex molecules not otherwise observable.

There are some drawbacks to molecular emission studies, however. First, analysis of the line excitation is very model dependent and can lead to significant systematic errors. Second, since spatial resolution is typically low (and varies from species to species), it is sometimes hard to discern whether emission from different species comes from the same location within a cloud. This makes comparisons among species difficult.

Molecular absorption line observations have some important advantages over emission-line studies. First, absorption from different species observed in the same line of sight are more likely to coexist spatially, thus reducing geometrical ambiguities and allowing more reliable interspecies comparisons. Second, because the unexcited molecules are observed directly, column density determinations are not as model dependent as for emission studies and hence more accurate. Third, some molecular species (notably, H_2 and C_2) are essentially unobservable in the radio because of the lack of a dipole moment. These species can sometimes be observed via electronic transitions in the ultraviolet (e.g., Shull & Beckwith 1982) or through rotational-vibrational transitions in the visible or infrared (e.g., Federman et al. 1994; Lacy et al. 1994). And finally, molecular abundances derived from absorption measures can easily be compared with line-of-sight bulk properties (e.g., extinction, polarization, and atomic abundances) which are also derived from absorption measures.

CO and C_2 have transitions at 2.3 μm and 8775 Å, respectively, which can be observed in absorption. The primary drawback to studying molecular absorption lines in the infrared (IR) is finding a suitable background star. The target must be bright in the IR yet fortuitously placed behind a substantial amount of absorbing material.

In our effort to find background sources for absorption-line studies in regions also accessible to emission-line studies, we have selected the target W40 IRS 1a, an OB star embedded within the radio source W40. This source appears well suited for our purposes; although dim in the visible ($V = 15.0$), it is bright in the IR ($K = 5.6$) and lies behind about 9 mag of extinction in V (A_V). W40 itself is a blister-type H II region breaking out of a local molecular cloud, about 400 pc away toward the Galactic center (Zeilik & Lada 1978; Crutcher & Chu 1982). A group of hot stars (most likely B class) is bathing the region with ionizing radiation; W40 IRS 2a (OS 2a) seems to be producing most of the energy (Smith et al. 1985). IRS 1a is brighter than 2a in the optical and near-IR, indicating somewhat greater extinction toward IRS 2a. Crutcher & Chu (1982) mapped ^{12}CO and ^{13}CO, HCO^+, HCN, and Hα emission toward W40, generating a comprehensive kinematic interpretation of the region. Vallée (1987), Vallée & MacLeod (1991, 1994), and Vallée, Guilloteau, & MacLeod (1992) have done extensive studies on the properties of the molecular cloud

and its interaction with the H II region using C II recombination lines, radio continuum emission, and CO emission. The existence of circumstellar dust shells around W40 IRS 1a, 2a, and 3a ($T \sim 250$–350 K and $M < 0.1\ M_\odot$) has been suggested based on broadband IR imaging and continuum measurements in the millimeter and submillimeter ranges (Smith et al. 1985; Vallée & MacLeod 1994).

Both CO and C_2 are important interstellar molecules. CO is the most abundant molecule in the ISM after molecular hydrogen and has a number of important roles. The CO emission lines at 2.6 mm and shorter not only are responsible for cooling molecular clouds but also serve as tracers for H_2 and dense molecular gas (e.g., Magnani & Onello 1995 and references therein). C_2 is much less abundant than CO and has been observed primarily in diffuse and translucent clouds (e.g., van Dishoeck & Black 1989; Lambert, Sheffer, & Federman 1995). Like H_2, C_2 has no dipole moment and hence no pure rotational spectrum. It is a very useful diagnostic of cloud physical conditions such as kinetic temperature, density, and radiation field intensity (van Dishoeck & Black 1982; van Dishoeck 1984). Both CO and C_2 are important to carbon chemistry everywhere in the ISM.

CO absorption at 2.3 μm ($v = 2$–0) has not been observed as frequently as the $v = 1$–0 band at 4.7 μm, most likely owing to the smaller transition probabilities. It is, however, easier to observe at 2.3 μm since the thermal background from the Earth's atmosphere is much lower than at 4.7 μm. Black & Willner (1984) and Black et al. (1990) used the lines at 2.3 μm to study the physical conditions and chemistry toward NGC 2024, NGC 2264, and AFGL 2591. Recently, Lacy et al. (1994) were able to observe both CO and H_2 absorption near 2.3 μm toward NGC 2024 IRS 2, yielding for the first time a direct measure of the H_2/CO ratio in a molecular cloud.

Absorption lines of C_2 have been used to address a number of problems in the ISM, including diffuse interstellar cloud chemistry (e.g., Lambert et al. 1995), carbon chemistry in translucent clouds (e.g., van Dishoeck & Black 1989), molecular cloud envelopes (e.g., Federman et al. 1994), and the line-of-sight structure toward ζ Oph (e.g., Crawford 1997). Federman et al. (1994) provide a good compilation of C_2 measurements up to 1992.

In this paper we report on absorption-line studies of CO and C_2 toward W40 IRS 1a. The line of sight is discussed in the next section. In § 3 we describe our observations and the results, and in § 4 we discuss their implication for the physical state of the material in this line of sight. The final section contains a brief summary of our conclusions.

2. LINE OF SIGHT

Very little is known about the interstellar sight line to W40 IRS 1a. Both Crutcher & Chu (1982) and Smith et al. (1985) infer $A_V \sim 9$. The average extinction due to diffuse material over 400 pc is about 0.6 mag (see Spitzer 1978, p. 155). Therefore the obscuring material is most likely local to the W40 region and more dense than the diffuse ISM. In addition, Crutcher & Chu (1982) found a molecular ^{13}CO component in front of the W40 H II region with $V_{\rm LSR} = 8$ km s^{-1}, $N_{\rm CO} \simeq 1.2 \times 10^{18}$ cm^{-2}, and $\log nT \sim 4$, further suggesting that the sight line passes through cold material, most likely associated with the neighboring molecular cloud.

The line of sight intersects at least three distinct physical regimes. As noted above, there appears to be some cold foreground material, perhaps associated with the nearby molecular cloud. Closer to W40 IRS 1a there must be a photon-dominated region (PDR) and, closer still, the W40 H II region itself. If W40 IRS 1a has a circumstellar dust shell, it is not clear what its effect on the CO and C_2 spectra might be. A warm dust shell might be associated with an elevated gas temperature and, hence, the appearance of high-J molecular rotational lines.

The H II region is roughly 0.9 pc across and has an electron density of 200 cm^{-3} (based on results in Crutcher & Chu 1982 and a distance of 400 pc). The column density of ionized hydrogen associated with the H II region should be about 3×10^{20} cm^{-2}, assuming spherical geometry and that all hydrogen is ionized. Using the relation of total hydrogen column density to extinction found in Bohlin, Savage, & Drake (1978), the H II region should contribute $A_V \sim 0.1$ mag to the line-of-sight extinction. This, of course, assumes a standard gas-to-dust ratio, which may not apply to H II regions in general. The contribution to A_V could increase or decrease depending primarily on the nature of any grain-destroying shocks which may have passed through the region. In either case, the H II region probably does not strongly contribute to the total extinction on the line of sight to W40 IRS 1a. In addition, molecules like CO and C_2 cannot survive in the harsh H II environment, so the H II region should not contribute to the line absorption for these molecules either.

There is almost surely a PDR on the line of sight to W40 IRS 1a, which could account for as much as $A_V \sim 10$, nearly the entire measured visual extinction (see Hollenbach 1990 for a good discussion). Hydrogen is expected to be neutral or molecular throughout the PDR. CO and perhaps C_2 cannot survive in the regions of the PDR closest to the H II region. The effect of dust in PDRs is poorly understood, and so a quantitative treatment of these regions in general is difficult.

In summary, CO and C_2 absorption lines should sample the cold material in the foreground, at least part of the PDR, and none of the H II region. A circumstellar dust shell, if it exists, would most likely only contribute to high-J molecular absorption. The visual extinction ($A_V \sim 9$) should arise almost entirely in the foreground material (which may be part of the local molecular cloud) and the PDR, although we note that the PDR could in theory produce all of the observed extinction.

3. DATA AND ANALYSIS FOR ^{12}CO AND C_2 TOWARD W40 IRS 1a

3.1. C_2 *Observations at* 8775 Å

The observations of W40 IRS 1a were obtained with the Cassegrain echelle spectrograph and the RCA CCD camera on the 4 m Mayall telescope at Kitt Peak National Observatory (KPNO) on the night of UT 1983 June 16. Two spectra, each of 1 hr duration, were recorded in the region of the $J = 2$–0 band of the Phillips system ($A\ ^1\Pi_u$–$X\ ^1\Sigma_g^+$) of C_2. The entire $J = 2$–0 band was contained in a single order with its center near 8775 Å and with a nominal reciprocal dispersion of 0.074 Å pixel^{-1} at the face of the CCD chip. Quartz lamp and thorium-argon spectra were obtained for flat-fielding and wavelength calibration. An 84 μm wide slit was employed, providing a nominal resolution of 0.15 Å,

which in turn corresponds to approximately 2 pixels on the chip.

The two consecutive 1 hr frames were co-added and averaged. Similarly, two separate flat-field frames were co-added and averaged, and the result was divided into the averaged stellar frame to produce the final photometric spectrum. Both flat-field and stellar frames were bias-corrected. The average of 15 bias frames was first subtracted from the flat-field and stellar frames, after which a second-order bias correction was accomplished by subtracting from the average stellar and flat-field frames the mean row biases obtained from the masked bias columns of each.

The final spectrum was extracted by collapsing the three columns along the slit direction which contained the maximum signal. This spectrum is shown in Figure 1. Spikes are due to cosmic-ray hits and possibly OH airglow lines. Rotational lines in all three branches (P, Q, and R) were identified, with the rotational quantum number J reaching as high as 12 for the Q branch. Unfortunately, there were problems with the wavelength calibration at the telescope, and we were not able to derive a precise measure for the radial velocities of the C_2 lines. Equivalent widths for these lines were determined using standard spectral reduction procedures in the NOAO/IRAF package, and column densities for each of the rotational levels were calculated from the rotational lines using a simple Gaussian curve of growth (see Spitzer 1978). Initially, the f-value derived by Erman et al. (1982) was used. Recently, the Phillips system transition probabilities have been refined (see Lambert et al. 1995 and references therein), and the column densities have been adjusted to reflect the new f-value derived by Lambert et al. (1995), $(1.23 \pm 0.16) \times 10^{-3}$. The data for each line and the column densities for each J are shown in Tables 1 and 2. Several of the lines exhibited effects of saturation, and an estimate of the Doppler constant (b) was derived by requiring that rotational lines originating from the same rotational energy level yield the same rotational population for that level. This method is a simple extension of the doublet ratio method used in the analysis of saturated atomic species. The best value for the Doppler constant was found to be 1.25 km s^{-1}. The $J = 12$ data are not included because of high uncertainty: only the Q12 line was observed, and it is very weak.

3.2. ^{12}CO *Observations at* 2.3 μm

The $v = 2$–0 rotational-vibrational lines for CO fall near 2.3 μm, within the K band. Since the oscillator strengths are smaller, the $v = 2$–0 lines are not as saturated as their $v = 1$–0 cousins at 4.7 μm. In addition, it is somewhat easier to observe at 2.3 μm, as the sky emission at 4.7 μm is much greater and more problematic. Contamination from stellar CO absorption should be negligible since W40 IRS 1a appears to be a hot O or B star, which would not allow stellar CO to survive (Crutcher & Chu 1982; Smith et al. 1985). Circumstellar gas and dust, if they exist, could affect the high-J molecular levels.

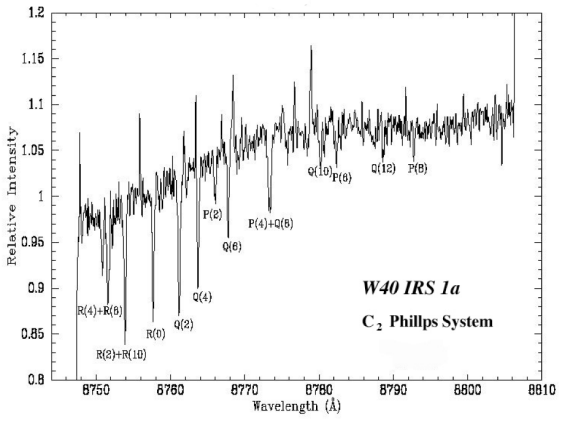

FIG. 1.—C_2 Phillips system toward W40 IRS 1a

TABLE 1

OBSERVED C_2 PHILLIPS SYSTEM LINES

Transition	Rest Wavelength (Å)	Equivalent Width (mÅ)
R0	8757.7	37.0 ± 3.0
R2	8753.9	52.5 ± 1.5[a]
Q2	8761.2	55.0 ± 5.0
P2.....	8766.0	18.0 ± 3.0
R4	8751.6	42.5 ± 7.5[b]
Q4	8763.7	36.0 ± 3.0
P4 + Q8.....	8773.3	43.0 ± 4.0
R6	8750.8	22.8 ± 3.0
Q6	8767.7	31.5 ± 4.5
P6.....	8782.3	12.5 ± 2.5
P8.....	8792.6	9.5 ± 2.0
Q10.....	8780.1	17.5 ± 2.5
Q12.....	8788.5	6.5 ± 2.0

[a] R2 and R10 are blended.
[b] R4 and R8 are blended.

Rotational-vibrational transitions at 2.3 μm for ^{12}CO were observed UT 1994 June 11 and UT 1997 July 21 using the CSHELL IR spectrometer at the NASA Infrared Telescope Facility (IRTF) on Mauna Kea. The IRTF is a 3 m primary, off-axis Cassegrain yielding $f/13.67$ at the spectrometer slit. The CSHELL is a cryogenically cooled echelle spectrometer with a 256 × 256 SBRC InSb detector array (Greene et al. 1993). We used the 0.″5 slit which gives $R \simeq 43{,}000$. Only the R0, R1, and R2 transitions were detected (Fig. 2) with upper limits placed on R3, R4, and R5. A summary of the observations is shown in Table 3. The data were obtained and reduced following typical IR observing procedures which we briefly summarize below.

Dark frames were co-added and subtracted from the flat-field image for each wavelength setting. W40 IRS 1a and the standard stars were observed in both the "A" and "B" beams (each beam places the spectrum in a different spatial location on the detector). Beam differences (A − B and B − A) were calculated to eliminate sky emission, then co-

TABLE 2

C_2 COLUMN DENSITIES

J	E_J/k (K)	N_J (10^{13} cm^{-2})
0	0.000	5.4 ± 0.8
2	15.635	19.8 ± 2.0
4	52.114	11.2 ± 1.6
6	109.430	9.2 ± 0.7
8	187.572	5.6 ± 0.7
10.....	286.526	4.1 ± 0.4
Total[a].....		70 ± 4

[a] Based on Boltzmann analysis for both 39 and 126 K.

TABLE 3

CSHELL ^{12}CO Observations Summary

Wavelength Range (μm)	^{12}CO Lines	Integration Time (minutes)	S/N[a]	Standard Stars
2.334–2.340	R3, R4, R5	25	90	BS 6714, 7110, 5 Aql
2.340–2.346	R0, R1, R2	25	90	Spica

[a] S/N for the regions surrounding the applicable lines.

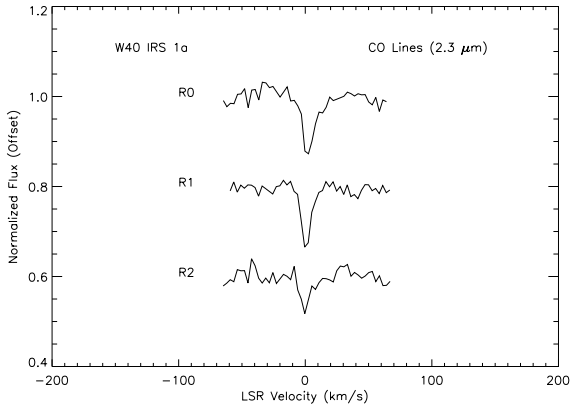

FIG. 2.—^{12}CO lines at 2.3 μm toward W40 IRS 1a. The continua for R1 and R2 are offset for clarity.

added and normalized using the flat field for the appropriate wavelength setting. Wavelength calibration was achieved using Ar, Kr, and Xe lamps with three lines per wavelength setting. One-dimensional spectra for W40 IRS 1a, the standard stars, and the calibration lamps were then extracted from the detector images using the APALL task in IRAF.

Once the wavelength solution was applied, telluric absorption features were identified in both the standard stars and W40 IRS 1a spectra. Telluric lines were eliminated from the W40 IRS 1a spectra using the IRAF task TELLURIC, which shifts and scales the standard star spectrum before dividing into the object spectrum. It is important to note that merely dividing the standard star spectrum into the object spectrum does not produce the *true* object spectrum without telluric features. To properly remove telluric features, one must generate an *expected* object spectrum, convolve it with the standard star spectrum, and compare with the actual observed object spectrum. Lacy et al. (1994) give a good discussion of this technique. We opted to merely divide, however, as our data quality did not warrant more sophisticated techniques.

The R0, R1, and R2 lines are shown in Figure 2. These lines imply $v_{\rm LSR} = 2 \pm 2$ km s^{-1}, in contrast with the 8 km s^{-1} foreground molecular material seen in emission (Crutcher & Chu 1982). Since emission-line data sample a large, beam-averaged area, and absorption lines just a pencil beam, we do not necessarily expect velocities derived from both to agree. We merely note that they are not wildly different.

$R = 43{,}000$ corresponds to a resolution of $\Delta v \simeq 7$ km s^{-1}. The R0, R1, and R2 lines all have FWHM ~ 8 km s^{-1} and hence are not well resolved. After continuum normalization, each line was directly integrated for equivalent width. Errors reflect continuum placement ambiguity and are of high confidence (2 σ). All the widths (along with transition information and errors) are given in Table 4. Widths for the R3, R4, and R5 lines are 2 σ upper limits based on the noise in the continuum at the expected line position.

TABLE 4

Observed ^{12}CO Lines ($v = 2$–0)

Transition	Rest Wavelength[a] (μm)	f-Value[b] ($\times 10^{-8}$)	Equivalent Width (mÅ)
R0	2.34530523	8.78	130 ± 20
R1	2.34326929	5.89	100 ± 10
R2	2.34127497	5.33	60 ± 17
R3	2.33932336	5.11	<20
R4	2.33741273	5.00	<20
R5	2.33554435	4.94	<20

[a] Mantz & Maillard 1974.
[b] Chackerian & Tipping 1983.

The equivalent width of any absorption line is dependent on the column density of the species and, if saturated, the velocity parameter b (see Spitzer 1978). We generated a model curve of growth (COG) using $b = 1.25$ km s^{-1}, as determined from the C_2 lines. Each ^{12}CO equivalent width was fitted to the COG independently and the column density for each rotational level (N_J) is given in Table 5. The R2 through R5 lines were clearly optically thin whereas the R0 and R1 lines were more optically thick, falling on the transition from the linear portion to the saturated part of the COG. If the b-value for CO is greater than 1.25 km s^{-1}, then the R0 and R1 lines become more optically thin and their abundances drop by 2 and 0.5×10^{17} cm^{-2}, respectively. Summing the abundances for each line gives a total column density of $N_{\rm CO} = (1.1 \pm 0.2) \times 10^{18}$ cm^{-2} (assuming ^{12}CO to be the dominant isotope). Depending on the excitation of the higher J levels, this value could be slightly too small, and if $b > 1.25$ km s^{-1}, then it would be too high. Our column density for CO is nearly identical to that inferred by Crutcher & Chu (1982) for the foreground, $N_{\rm CO} \simeq 1.2 \times 10^{18}$ cm^{-2}.

TABLE 5

^{12}CO Column Densities

J	E_J/k (K)	N_J (10^{17} cm^{-2})
0	0	5.0 ± 2.0
1	5.532	4.0 ± 1.5
2	16.60	2.2 ± 0.7
3	33.19	<0.8
4	55.32	<0.8
5	82.98	<0.8
Total.....		11 ± 2

3.3. CO *Ice Band at* 4.7 μm

In an effort to detect the CO ice band at 4.7 μm we made observations with moderate spectral resolution at the United Kingdom Infrared Telescope (UKIRT) using the CGS4 on 1998 August 19. All observations were carried out while nodding along the slit to remove atmospheric emission. The total integration time on W40 IRS 1a was 11.2 minutes at an average air mass of 1.45. The spectrum for W40 IRS 1a was ratioed by BS 7236 (B9 V) to remove telluric absorption features. The signal-to-noise ratio (S/N) is $\sim$44 at 4.67 μm and no CO ice feature is apparent. An upper limit for the optical depth of the band is $\tau_{4.67} < 0.02$ (2 σ), implying $N_{\rm CO}({\rm ice}) < 10^{16}$ cm^{-2} (Tielens & Allamandola 1987). The depletion of CO into icy mantles for the W40 IRS 1a sight line must be less than 1%.

4. DISCUSSION

4.1. *Excitation Conditions and the Foreground Cloud Physical Properties*

We have three basic diagnostics for the temperature and density toward W40 IRS 1a. The ^{13}CO emission data imply $\log nT \sim 4$, much lower than the nearby molecular cloud, $\log nT \sim 6.5$ (Crutcher & Chu 1982). Excitation conditions can also be derived from the rotational populations of CO and C_2.

The rotational level populations of the C_2 Phillips system ($v = 0$, J) are attained via radiative pumping. Lifetimes of these levels are so long that collisions and upward electronic transitions are the most important depopulation mechanisms. Hence the rotational populations reflect the competition between pumping and collisions and are nonthermal in general (van Dishoeck & Black 1982). For densities greater than 100 cm^{-3}, the $J = 0$ and $J = 2$ levels are very nearly thermal. Otherwise, the populations depend on the thermal temperature, T, and the radiation parameter, $n_c\,\sigma/I_R$, where n_c is the collision partner density [usually $n({\rm H}) + n({\rm H}_2)$], σ is the effective cross section for collisional de-excitation, and I_R is the scaling factor for the radiation field in the far-red (van Dishoeck & Black 1982).

Total molecular abundance and excitation temperatures were calculated from models which fit a Maxwell-Boltzmann population distribution to the observed rotational level abundances. As had been found for other relatively dense clouds (Lutz & Crutcher 1983), the rotational abundances could not be fitted with a single temperature distribution, presumably as a result of radiative pumping (Chaffee et al. 1980; van Dishoeck & Black 1982). Consequently, we fit these data with a two-temperature model used by Lutz & Crutcher (1983): J levels 4 through 10 were fitted with an excitation temperature ($T_{\rm ex}$) of 126 K, which we associate with the effects of radiative pumping. After correcting the populations in $J = 0$ and 2 for the contributions from the 126 K population distribution, we derived a $J = 2/J = 0$ excitation temperature of 39 K, which we associate with the thermal distribution of the gas. The resulting total column density of C_2 toward W40 IRS 1a is $(7.0 \pm 0.4) \times 10^{14}$ cm^{-2}, based on a Boltzmann distribution for both temperatures. This is the highest column density of C_2 yet seen in absorption. Figure 3 shows the final fits.

In comparing the results for W40 IRS 1a to the radiative pumping models calculated by van Dishoeck (1984), we found that they are best characterized by her model with a kinetic temperature of 40 K and a radiation parameter, $n_c\,\sigma/I_R$ of 5.27×10^{-14}. Assuming $I_R = 1$, $\sigma \sim 2 \times 10^{-16}$ cm^2 (van Dishoeck & Black 1989), and that hydrogen (H I + H_2) is the only important collision partner, we get $n_{\rm H} \sim 250$ cm^{-3} for the W40 IRS 1a sight line. Since the value of σ is not known to better than a factor of 2 (van Dishoeck & Black 1989), our value for $n_{\rm H}$ is equally imprecise. In addition, for an enhanced (or depleted) radiation field, the estimated collision (hydrogen) density would scale accordingly.

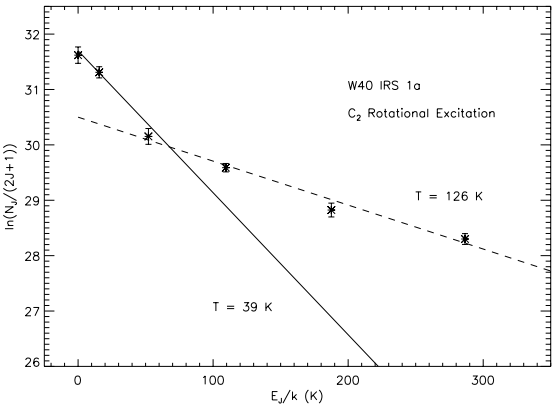

FIG. 3.—Boltzmann plot for rotational levels of C_2: two-temperature model, 39 K (*solid line*) and 126 K (*dashed line*).

Rotational transitions of CO are primarily excited by collisions with hydrogen. De-excitation can occur via collisions with hydrogen or by spontaneous line emission. The critical density at which collisions begin to overtake spontaneous emission is around 3000 cm^{-3}. More detailed studies of the excitation, photodissociation, and chemistry have been conducted by van Dishoeck & Black (1988) and Warin, Benayoun, & Viala (1996). In general, it is found that the rotational populations of CO are subthermal except for the first few levels in dense cases (Warin et al. 1996). Hence the assumption of LTE will almost always produce excitation temperatures which underestimate the actual thermal temperature ($T_{\rm ex} < T_{\rm kin}$). Recent work by Wannier, Penprase, & Andersson (1997) suggests that the dominant form of CO excitation in diffuse and translucent clouds can be line emission from nearby molecular clouds, if the clouds have similar velocity vectors.

As a start, we constructed a Boltzmann plot for the ^{12}CO data (Fig. 4). Fitting the temperature to all lines gives $T_{\rm ex} =$ 7 K. This value is similar to that found by Cruther & Chu (1982), but it is important to note that the excitation temperatures for ^{13}CO and ^{12}CO are different in general (Warin et al. 1996). Since the thermal temperature is greater than the CO rotational temperature in general, $T_{\rm kin} > 7$ K, which is consistent with the C_2 analysis. Warin et al. (1996) have constructed models of CO excitation for the dense, translucent, and diffuse cloud regimes, including UV photodissociation. These models show very clearly that the excitation temperature is much lower than the thermal temperature for diffuse and translucent clouds. The excitation of CO in dense clouds is nearly thermal and $T_{\rm ex} = T_{\rm kin}$. If we assume that the cloud(s) toward W40 IRS 1a are dense, then $T_{\rm kin} \simeq 7$ K. For diffuse and translucent clouds, the level populations observed can be scaled (see § 4.2 of Warin et al. 1996) to derive "pseudo-LTE" rotational populations, i.e., representative LTE populations for the actual thermal temperature of the gas. A slope can be fitted

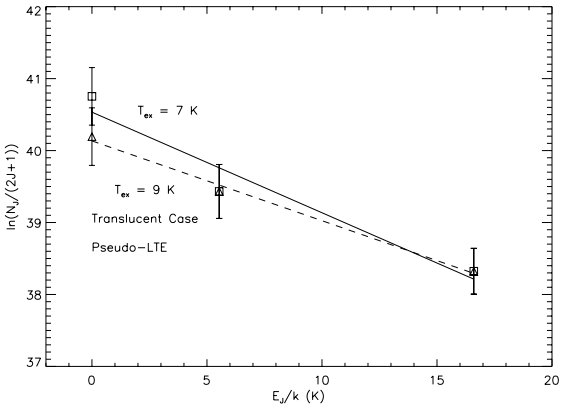

FIG. 4.—Boltzmann plot for rotational levels of ^{12}CO. Squares are observed column densities from Table 5 with $T_{ex} = 7$ K (*solid line*). Triangles are pseudo-LTE populations assuming material on the line of sight is translucent in nature with temperature fit ($T_{ex} = 9$ K, *dashed line*). See § 4.1 for discussion.

to these populations and a thermal temperature inferred. If the cloud(s) toward W40 IRS 1a are translucent, then the R0 population is reduced by ~ 1.75 (changes in R1 and R2 happen to be negligible). The resulting populations imply $T_{kin} \simeq 9$ K (see Fig. 4), which still does not agree with the C_2 analysis. It is not clear, however, that the models constructed by Warin et al. (1996) apply to our line of sight: the UV field is probably higher than normal near W40, and it seems very likely that there are multiple clouds on the sight line.

Since the cloud(s) on the W40 IRS 1a line of sight are very near the W40 molecular cloud, and the LSR velocities of both are similar (5 and 8 km s^{-1}), the excitation for ^{12}CO may be at least partially radiative. Comparing to models constructed by Wannier et al. (1997) it is apparent that our $T_{ex} = 7$ K is degenerate: it can be accounted for by many combinations of radiative excitation, collision partner density, and kinetic temperature. The C_2 excitation conditions can help constrain those for ^{12}CO. If we assume $T_{kin} \simeq 40$ K, the density of the gas can range from 0 to 450 cm^{-3}, depending on the efficiency of radiative excitation. Collisional excitation becomes dominant as n approaches 450 cm^{-3} (which we use as an upper limit). If we further assume $n \sim 250$ cm^{-3} (as indicated by the C_2 data), then the excitation of CO can only be explained by collisional and radiative processes combined.

A summary of the W40 IRS 1a sight-line cloud physical properties based on the CO and C_2 data in this paper, as well as the CO emission study by Crutcher & Chu (1982), is given in Table 6. As discussed in § 2, we assume that nearly all of the absorption on this line of sight arises in one cloud complex (single or multiple components) local to the W40 region, since it is only 400 pc distant (i.e., the cloud[s] cannot be diffuse). The physical conditions are best determined by C_2: $n \sim 250$ cm^{-3} and $T \simeq 40$ K. The CO emission and absorption values and limits agree very well. The cloud(s) is (are) clearly not dense enough to be considered molecular but could be considered translucent. Translucent lines of sight typically have $A_V = 2$–5 and can be studied via both absorption lines (UV, optical, and/or IR) and radio emission lines. In addition, translucent material is expected in the outer envelopes of molecular clouds (van Dishoeck & Black 1989). We postulate that the W40 IRS 1a sight line is composed of multiple translucent components associated with the W40 molecular cloud.

4.2. *Molecular Abundances*

CO and C_2 abundances have been determined jointly for a number of sight lines, a sample of which is shown in Table 7. W40 IRS 1a is one of few sight lines allowing a direct comparison of CO and C_2 in *absorption*. The abundance ratio we derive is CO/$C_2 = 1600 \pm 600$ (2 σ). The depletion of CO onto dust is negligible (<1%), in view of our failure to detect CO ice, but the C_2 depletion has not been assessed. Note that the CO/C_2 ratio increases from diffuse to translucent and molecular regimes indicating (to first order) that the formation/destruction rates favor CO over C_2 as cloud type changes. This may merely be due to self-shielding of CO, but other processes may also be in action: the data are not yet precise enough to tell.

Assuming all hydrogen is molecular, we can estimate the amount of H_2 on the W40 IRS 1a line of sight from N_{CO}. Using an H_2/CO ratio of 3700^{+3100}_{-2700} (based on the direct comparison of H_2 and CO IR absorption lines toward NGC 2024 IRS 2 [$A_V = 21.5 \pm 5$]; Lacy et al. 1994), we find $N_{H_2} = 4.4^{+3.8}_{-3.2} \times 10^{21}$ cm^{-2}. The H_2/CO ratio is derived from a direct comparison of weak absorption lines and hence should be reliable, but it is based on only one data point: NGC 2024 IRS 2. If this sight line is abnormal in any way, then the ratio does not necessarily apply to other lines of sight such as W40 IRS 1a.

4.3. *Dust Indicators*

The A_V calculated by Crutcher & Chu (1982) and Smith et al. (1985) assumes a "normal" extinction law ($R_V \sim 3$), which may be incorrect. The ratio of visual to selective extinction, R_V, is a grain size distribution indicator (Cardelli, Clayton, & Mathis 1989): $R_V < 3$ implies an abundance of small grains compared with the typical size distribution, whereas $R_V > 3$ implies that larger grains

TABLE 6

W40 IRS 1a SIGHT-LINE PHYSICAL PROPERTIES

Species	V_{LSR} (km s^{-1})	b (km s^{-1})	N (cm^{-2})	T_{ex} (K)	n_H[c] (cm^{-3})	log nT
C_2	...	1.25	$(7.0 \pm 0.4) \times 10^{14}$	39, 126[b]	$\sim$250	...
^{13}CO emission[a].....	8	...	1.2×10^{18}	...	...	$\sim$4
^{12}CO	2 ± 2	...	$(1.1 \pm 0.2) \times 10^{18}$	>7	<450[d]	...

[a] Crutcher & Chu 1982.
[b] $T = 126$ K component due to radiative pumping.
[c] H + H_2.
[d] Assuming $T \simeq 40$ K, see § 4.1.

TABLE 7

SIGHT LINES WITH CO AND C_2 OBSERVATIONS

Sight Line	N_{CO} [a] (cm^{-2})	N_{C_2} [b] (cm^{-2})	CO/C_2	Cloud Type[c]	A_V	References
W40 IRS 1a.....	1.1 ± 0.2(18)	7.0 ± 0.4(14)	1600 ± 600	T	7.5–12.5	This work
Cyg OB2-12.....	2(16)	3.0 ± 0.2(14)	67 ± 5	D	~10	1, 2
HD 94413	0.7–1.2(16)[d]	2.8(13)	250–430	T	2.4	3
HD 154368.....	0.6–1.5(16)[d]	4.6(13)	130–330	T	2.5	3
HD 169454.....	0.55–1.8(16)[d]	5.6(13)	100–320	T	3.3	3
o Per.....	1.1(15)	1.8(13)	60	D	0.9	4
HD 27778	2.5(16)	3.0(13)	830	T	1.2	4
ρ Oph A.....	1.9(15)	2.1(13)	90	T	1.4	4, 7
ζ Oph.....	2.3(15)	1.79 ± 0.06(13)	130	D/T	0.96	4
20 Aql	3(15)	4.2(13)	71	D/T	0.99	4
HD 207198.....	2.6(15)	2.4(13)	110	T	1.9	4
HD 21483	1.0(18)	7.4(13)	100–10^5	T	1.7	4
ζ Per	1.2(15)	2.8(13)	43	D/T	1.0	4
X Per	5.0(15)	4.2(13)	120	T	1.4	4
HD 26571	6.0(16)	8.8(13)	680	D/T	0.9	4
AE Aur	1.3(15)	4.6(13)	28	T	1.6	4
HD 110432.....	1.0(15)	2.4(13)	42	T	1.2	4
π Sco	1.0(12)	<1.0(12)	>1	D	0.19	5
β^1 Sco	1.2(13)	<1.0(12)	>12	D	0.62	5
ω^1 Sco	4.0(13)	<2.0(12)	>23	D	0.68	5
χ Oph.....	3.0(14)	2.8(13)	11	T	1.2	4
9 Cep	1.7(13)	1.0(13)	2	D[e]	1.5	4
HD 210121.....	3.0(15)[d]	5.2(13)	58	T (high latitude)	~1	6
λ Cep	1.4(15)	1.4(13)	100	D[e]	1.8	4

NOTE.—$X(Y) = X \times 10^Y$.

[a] All column densities derived from UV or IR absorption lines except where noted.

[b] Where appropriate, the column density for C_2 has been adjusted to account for the new *f*-value derived by Lambert, Sheffer, & Federman 1995.

[c] Cloud types: D = diffuse, T = translucent.

[d] From millimeter emission lines.

[e] Possibly more than one cloud.

REFERENCES.—(1) McCall et al. 1998; (2) Lutz & Crutcher 1983; (3) Gredel, van Dishoeck, & Black 1994; (4) Federman et al. 1994 and references therein; (5) Lambert, Sheffer, & Federman 1995; (6) Gredel et al. 1992; (7) Federman et al. 1999.

dominate the extinction. As interstellar clouds collapse the dust grains tend to agglomerate, eliminating the smaller particles (Jura 1980). If the line of sight toward W40 IRS 1a does indeed sample the edge of a molecular cloud, then we would expect a population of larger grains and $3 < R_V < 5$. Smith et al. (1985) found $B-V = 2.2$ for W40 IRS 1a, and assuming it is an OB star, $E_{B-V} \simeq 2.5$. For $R_V = 3$–5, we get a range in A_V of 7.5–12.5, which agrees with the previous work by Crutcher & Chu (1982) and Smith et al. (1985).

Our calculated value of A_V can be used to predict the amount of CO expected toward W40 IRS 1a. As discussed in § 2, however, the extinction and CO absorption may not be well correlated in the PDR, leading us to slightly *overestimate* N_{CO} based on A_V. Conversely, most studies of the CO/A_V ratio have not addressed the depletion of CO into ice mantles (which may be as high as 40%; Chiar et al. 1995). Since CO is almost entirely in the gas phase for the W40 IRS 1a line of sight, these studies will *underestimate* the predicted CO column density. Using radio maps, spectroscopic data, and star counts in the Taurus and ρ Oph clouds, Frerking, Langer, & Wilson (1982) found

$$N(C^{18}O) = 1.7 \times 10^{14}(A_V - 1.3) \quad (1)$$

for N in units of cm^{-2} and $4 < A_V < 21$. This relation predicts $N_{CO} = (0.5\text{–}1.0) \times 10^{18}$ cm^{-2} [with $N(CO)/N(C^{18}O) = 490$] for our line of sight, very nearly the same as we have measured. Interestingly, it may be that the PDR effect nearly balances the depletion effect.

There is no strong correlation between C_2 and E_{B-V} (van Dishoeck & Black 1989), although other dust indicators have not been investigated. The lack of correlation may be due to the fact that many of the stars included in C_2 absorption studies to date have been distant supergiants where some of the sight-line extinction is caused by diffuse clouds, which lack abundant C_2.

Comparing the W40 IRS 1a sight line with others in Table 7, it is apparent that CO and C_2 generally increase with A_V, but the data are too scattered to draw any strong conclusions.

The measurement of CO and C_2 absorption toward Cyg OB2-12, the classic diffuse cloud line of sight with $A_V \simeq 10$, is quite interesting. Lutz & Crutcher (1983) found $N_{C_2} = (3.0 \pm 0.2) \times 10^{14}$ cm^{-2} (adjusted for new Phillips system *f*-values in Lambert et al. 1995), about half of the abundance on the W40 IRS 1a sight line. Recently, McCall et al. (1998) measured CO IR absorption toward Cyg OB2-12 yielding $N_{CO} = 2 \times 10^{16}$ cm^{-2}, a factor of 60 less than what we find for W40 IRS 1a over nearly the same total visual extinction. The 4.7 μm CO ice feature is not seen on this line of sight; therefore, depletion of CO onto ice mantles cannot readily explain the discrepancy. This clearly shows that the gaseous CO-to-dust ratio changes from diffuse to denser environments.

As an interesting side note, we have compared the total hydrogen column density (assuming all of it to be molecular) for both W40 IRS 1a and NGC 2024 IRS 2 with

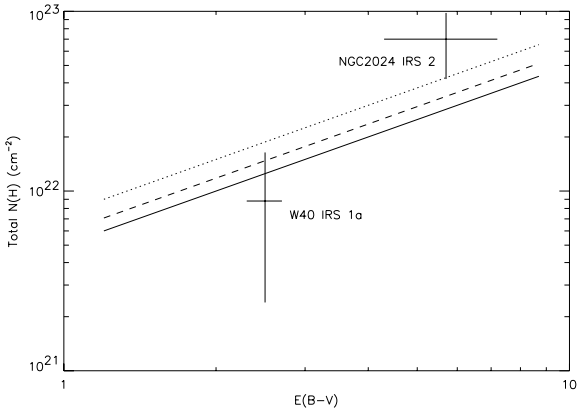

FIG. 5.—Correlation of reddening and total hydrogen column density. *Solid line*: "intercloud" relationship extrapolation from Bohlin, Savage, & Drake (1978); *dashed line*: "cloud" extrapolation; *dotted line*: relationship found by Dickman (1978). The total H column density for both W40 IRS 1a and NGC 2024 IRS 2 assumes all hydrogen is molecular. See § 4.3 for further discussion.

the hydrogen/reddening correlations found by Bohlin et al. (1978) and Dickman (1978) (Fig. 5). The E_{B-V} for NGC 2024 IRS 2 assumes $A_V = 21$ (Lacy et al. 1994; Jiang, Perrier, & Lena 1984) and R_V ranging from 3 to 5. The correlations ("intercloud" and "cloud") from Bohlin et al. (1978) are based on Lyα absorption for lightly reddened sight lines with $E_{B-V} < 0.6$, whereas the relation from Dickman (1978), derived from CO emission, is good to $E_{B-V} \sim 3$. In Figure 5 we have extrapolated out to $E_{B-V} = 10$. The data from W40 IRS 1a and NGC 2024 IRS2 agree with the extrapolated relations surprisingly well, within factors of 2 or so.

5. CONCLUSIONS

We have used ^{12}CO and C_2 IR and visible absorption lines to investigate the line of sight toward W40 IRS 1a. The C_2 data were obtained at the 4 m Mayall Telescope at KPNO and the ^{12}CO data from the CSHELL on the IRTF. The CO ice band at 4.7 μm was not detected. This sight line is clearly much more dense than diffuse, based on $A_V \sim 9$ and a distance of only 400 pc (we calculate a range in A_V of 7.5–12.5, assuming a population of large grains). Our ^{12}CO and C_2 data show the following:

1. The C_2 excitation conditions, $T \simeq 40$ K and $n \sim 250$ cm^{-3}, agree with limits determined from CO emission and absorption. Since the A_V is large and both absorption and emission measures are available, we postulate that the W40 IRS 1a sight line has multiple translucent components.
2. The nondetection of CO ice indicates a CO depletion of $\delta < 1\%$.
3. Comparing with other sight lines in Table 7, we find an overall increase in N_{CO} and N_{C_2} with increasing A_V. The data, however, are too scattered to draw any further conclusions at this point. The ratio of CO to C_2 appears to increase from diffuse to translucent and molecular sight lines probably due to the self-shielding of CO.
4. The column density of CO toward W40 IRS 1a is $\sim$60 times that found for Cyg OB2-12, the classic diffuse line of sight (McCall et al. 1998), despite very similar A_V values. This is not a depletion effect and suggests that the CO-to-dust ratio changes from diffuse to dense environments.
5. Finally, the relationship of hydrogen column density to interstellar reddening (Bohlin et al. 1978; Dickman 1978) was found to be roughly consistent with recent data out to $E_{B-V} \sim 10$ (Fig. 5). Contrary to the CO-to-dust ratio, the hydrogen-to-dust ratio appears to be valid from diffuse to dense regimes.

This research was supported by NASA Graduate Student Research Program grant (NGT5-50032) to R. Y. Shuping and NASA grant NAG5-4184 to T. P. Snow. We would like to thank the staff and operators at KPNO, the IRTF (J. Rayner), and the UKIRT (T. Kerr) for their help and tireless duty through the night. Many thanks to J. Black and the referee S. Federman, whose comments and suggestions greatly improved the content and quality of this paper. B. L. Lutz would like to thank K. Sheth, who carried out the curve-of-growth analysis and temperature fits for the C_2 lines. R. Y. Shuping would like to thank B.-G. Andersson, J. H. Lacy, and D. Jansen for their helpful input, and also D. E. Schutz for useful conversations and support.

REFERENCES

Black, J. H., van Dishoeck, E. F., Willner, S. P., & Woods, R. C. 1990, ApJ, 358, 459
Black, J. H., & Willner, S. P. 1984, ApJ, 279, 673
Bohlin, R. C., Savage, B. D., & Drake, J. F. 1978, ApJ, 224, 132
Cardelli, J. A., Clayton, G. C., & Mathis, J. S. 1989, ApJ, 345, 245
Chackerian, C., & Tipping, R. H. 1983, J. Mol. Spectrosc., 99, 431
Chaffee, F. H., Jr., Lutz, B. L., Black, J. H., Vanden Bout, P. A., & Snell, R. L. 1980, ApJ, 236, 474
Chiar, J. E., Adamson, A. J., Kerr, T. H., & Whittet, D. C. B. 1995, ApJ, 455, 234
Crawford, I. A. 1997, MNRAS, 290, 41
Crutcher, R. M., & Chu, Y. 1982, in Regions of Recent Star Formation, ed. R. S. Roger & P. E. Dewdney (Dordrecht: Reidel), 53
Dickman, R. L. 1978, ApJS, 37, 407
Erman, P., Lambert, D. L., Larsson, M., & Mannfors, B. 1982, ApJ, 253, 983
Federman, S. R., Lambert, D. L., van Dishoeck, E. F., Andersson, B.-G., & Zsargo, J. 1999, in preparation
Federman, S. R., Strom, C. J., Lambert, D. L., Cardelli, J. A., Smith, V. V., & Joseph, C. L. 1994, ApJ, 424, 772
Frerking, M. A., Langer, W. D., & Wilson, R. W. 1982, ApJ, 262, 590
Gredel, R., van Dishoeck, E. F., & Black, J. H. 1994, A&A, 285, 300
Gredel, R., van Dishoeck, E. F., de Vries, C. P., & Black, J. H. 1992, A&A, 257, 245
Greene, T. P., Tokunaga, A. T., Toomey, D. W., & Carr, J. S. 1993, Proc. SPIE, 1946, 313
Hollenbach, D. J. 1990, in ASP Conf. Ser. 12, The Evolution of the Interstellar Medium, ed. L. Blitz (San Francisco: ASP), 167
Jiang, D. R., Perrier, C., & Lena, P. 1984, A&A, 135, 249
Jura, M. 1980, ApJ, 235, 63
Lacy, J. H., Knacke, R., Geballe, T. R., & Tokunaga, A. T. 1994, ApJ, 428, L69
Lambert, D. L., Sheffer, Y., & Federman, S. R. 1995, ApJ, 438, 740
Lutz, B. L., & Crutcher, R. M. 1983, ApJ, 271, L101
Magnani, L., & Onello, J. S. 1995, ApJ, 443, 169
Mantz, A. W., & Maillard, J.-P. 1974, J. Mol. Spectrosc., 53, 466
McCall, B. J., Geballe, T. R., Hinkle, K. H., & Oka, T. 1998, Science, 279, 1910
Shull, J. M., & Beckwith, S. 1982, ARA&A, 20, 163
Smith, J., Bentley, A., Castelaz, M., Gehrz, R. D., Grasdalen, G. L., & Hackwell, J. A. 1985, ApJ, 291, 571
Spitzer, L., Jr. 1978, Physical Processes in the Interstellar Medium (New York: Wiley)
Tielens, A. G. G. M., & Allamandola, L. J. 1987, in Physical Processes in Interstellar Clouds, ed. G. E. Morfill & M. Scholer (Dordrecht: Reidel), 333
Vallée, J. P. 1987, A&A, 178, 237
Vallée, J. P., Guilloteau, S., & MacLeod, J. M. 1992, A&A, 266, 520

Vallée, J. P., & MacLeod, J. M. 1991, A&A, 250, 143
———. 1994, AJ, 108, 998
van Dishoeck, E. F. 1984, Ph.D. thesis, Leiden Univ.
van Dishoeck, E. F., & Black, J. H. 1982, ApJ, 258, 533
———. 1988, ApJ, 334, 771
van Dishoeck, E. F., & Black, J. H. 1989, ApJ, 340, 273
Wannier, P., Penprase, B. E., & Andersson, B.-G. 1997, ApJ, 487, L165
Warin, S., Benayoun, J. J., & Viala, Y. P. 1996, A&A, 308, 535
Zeilik, M., & Lada, C. J. 1978, ApJ, 222, 896